# HADRON CORRELATIONS
# AT ENERGIES FROM GeV TO TeV

## W. Kittel

Institute for Mathematics, Astrophysics and Particle Physics
Radboud University Nijmegen/Nikhef, Nijmegen, The Netherlands

*Dedicated to Andrzej Bialas in honour of his 80th birthday*

One of the central issues in High Energy Physics is the close interchange between Theory and Experiment. Ever since I know Andrzej Bialas, I know him as one of the theorists most interested in experimental data. This has naturally led to continuous fruitful contacts. Even though we have been working somehow together since about 1968, we so far have only one single publication in common. This was back in 1969 and it was on means to efficiently study what we then called (exclusive) Multihadron Final States. At that time, this meant 3- or at best 4-particle final states of two-hadron collisions at c.m.s. energies of some 4 GeV (not TeV!). The field of multiparticle dynamics was, in fact, the domain of Polish high-energy physicists. The first of a very successful (and still lasting) series of annual International Symposia on Multiparticle Dynamics was organized in Paris in 1970, but essentially by Polish physicists. Andrzej himself was not attending, but it was him who organized the third in these series in (of course) Zakopane. Since heavy-ion collisions, another field of major interest for Andrzej, will be covered by others, I here will restrict myself mainly to the collisions of two elementary particles.

## 1. Exclusive longitudinal phase-space analysis and its variables

One of our common interests at that time was the so-called Longitudinal Phase-Space (LPS) Analysis of 3- and 4- or even 5-particle final states and I will first try to recall the ideas behind that.

The most complete way to study a so-called exclusive reaction of multiplicity $n$

$$A + B \longrightarrow C_1 + C_2 + \cdots + C_n \tag{1}$$

is to look at the differential distribution of its matrix element in full phase space. This, however, requires a $(3n - 4)$-dimensional analysis $((3n - 5)$-dimensional if the incident particles are unpolarized) and becomes increasingly impossible with increasing $n$.

Nature helps: at low c.m.s. energies, the vast majority of collisions is "soft", *i.e.* leads to low transverse (with respect to the collision axis) momenta of final-state particles, largely independent of the nature of the particle, the multiplicity $n$ and the c.m.s. energy $s^{1/2}$. On the other hand, longitudinal (along the collision axis) momenta are unlimited (*i.e.* limited only by phase space) and depend strongly on the nature of the particle, the multiplicity and the energy.

In elastic and other two-particle production collisions, one is used to distinguish between forward and backward scattering. An extension of this classification to multiparticle final states is an analysis in just longitudinal phase space (LPS) [1, 2]. Then, each individual reaction of type (1) is represented by a point with coordinates $(p_{\parallel 1}, \ldots, p_{\parallel n})$ in a now only $n$-dimensional Euclidean space $S_n$. Conservation of longitudinal momentum in the c.m.s.,

$$\sum_{n}^{} p_{\parallel i}^* = 0 \,, \tag{2}$$

defines LPS as an $(n - 1)$-dimensional hyperplane $L_{n-1}$. Furthermore, because of conservation of c.m.s. energy $s^{1/2}$

$$\sum_{i=1}^{n} \left( m_i^2 + p_{\mathrm{T}i}^2 + p_{\parallel i}^{*2} \right)^{1/2} = s^{1/2} \,. \tag{3}$$

All points with equal transverse momentum $|p_{\mathrm{T}i}|$ lie on an $(n - 2)$-dimensional hypersurface $K_{n-2}$ defined by (3). For the case of a transverse mass $m_{\mathrm{T}i} = (m_i^2 + p_{\mathrm{T}i}^2)^{1/2} = 0$, (3) reduces to

$$\sum_{i=1}^{n} \left| p_{\parallel i}^* \right| = s^{1/2} \tag{4}$$

and defines a regular polyhedron $H_{n-2}$. For $n = 3$, this is the Van Hove Hexagon shown in Fig. 1 together with the one-dimensional manifold $K_1$. For $n = 4$, the polyhedron $H_2$ is the cuboctrahedron celebrated in Fig. 2.

A typical three-particle distribution in LPS for the final state of reaction

$$\pi^- p \to p \pi^- \pi^0 \tag{5}$$

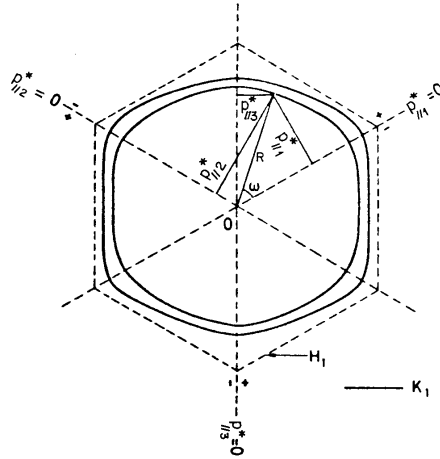at an incident lab momentum of 16 GeV/$c$ is given in Fig. 3 [3].

Fig. 1. Longitudinal phase-space plot (Van Hove Hexagon) for the final state $\pi\pi N$ at the c.m.s. energy of $s^{1/2} = 4$ GeV. The innermost solid line is $K_1$ for transverse momenta of 0.4, 0.4, and 0.5 GeV/$c$, respectively, while the outer one is $K_1$ for vanishing transverse momenta. The dashed line represents the hexagon $H_1$ [1].



Fig. 2. The polyhedron $H_2$ for a four-particle final state (cartoon by R. Sosnowski).

The distribution of (5) against the angle $\omega$ is given in Fig. 4, before and after correcting for phase-space effects (sub-figure (a) and (b), respectively). According to the definition in Fig. 1, the $\omega$ region considered ($60° < \omega < 120°$) corresponds to the hemisphere of LPS in which the proton is backward in the c.m.s. The $\pi^0$ is taken to be longitudinally at "rest" at $\omega = 120°$, the $\pi^-$ at $\omega = 180°$. Peaks in the (model independent!) experimental data (histograms) indicate strong correlations between particles in the final state, in particular in the region of $60 < \omega < 120°$.
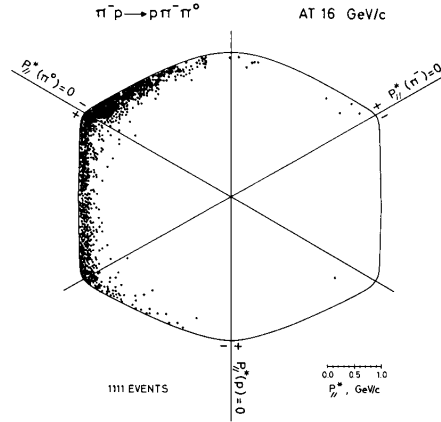
Fig. 3. Distribution of final-state points for the reaction $\pi^- \to \pi^- \pi^0 p$ at incident lab momentum of 16 GeV/$c$ [3].

As a demonstration of how one can use LPS to test the success of theoretical models, the so-called CŁA model [4] of that time was used. It is a Reggeized form of a multiperipheral model, in which the amplitude is treated as an incoherent sum of contributions from various multiperipheral graphs. For the reaction studied in Fig. 4, they are given in sub-figure (c) together with their contributions. The solid line in (a) and (b) corresponds to their incoherent sum. After exclusion of a sharp $\rho$-resonance, the model can describe the overall distribution of Fig. 4 surprisingly well. From the contribution of the graphs in sub-figure (c), we can see that vacuum exchange, commonly called $\mathbb{P}$(omeron) exchange, on the upper vertex essentially determines the shape of the distribution.

Turning back to a model-independent data analysis, we investigate the energy dependence of the distribution and its shape in Fig. 5 according to its parametrization $\sigma(p_{\text{lab}}) \propto p_{\text{lab}}^{-N}$. As shown in sub-figure (b), $N$ is indeed close to zero for $60° < \omega < 120°$, in agreement with $\mathbb{P}$ exchange (diffraction dissociation) in that region [5].

Where, however, is the $\Delta$ resonance? Unlike the incident proton, it has isospin $I = {}^3\!/_2$ and cannot, therefore, be produced via vacuum exchange.

One way to look for it is the so-called prism plot [6] ingeniously combining the advantages of the angle $\omega$ along the $z$-axis with the subsystem masses given in a Fabri–Dalitz plot (triangle) at the basis (Figs. 6 and 7). The separation into individual mechanisms, each corresponding to a straight section of the tube within the prism, is better than in its projection onto the $z$-axis or the basis in the $xy$-plane. The mass of the $(p\pi^+)$-subsystem is plotted in Fig. 8, for all events (sub-figure (a)) and for events in the corresponding section of the tube (sub-figure (b)). In the latter, the $\Delta^{++}$ is well-separated from the background still present in (a).
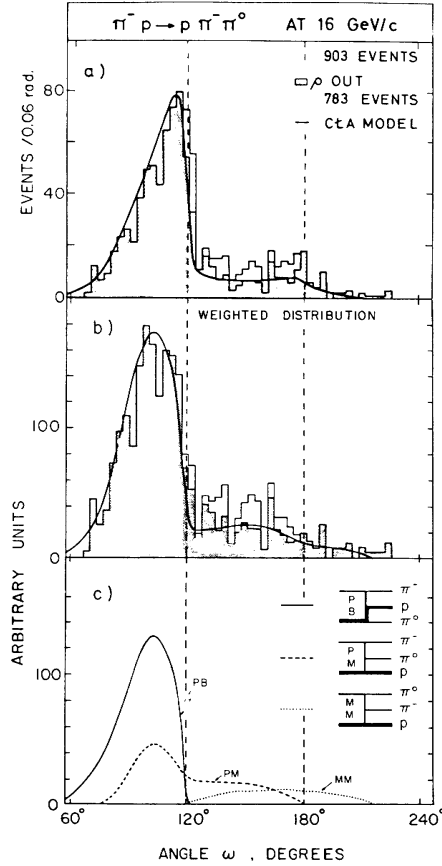
Fig. 4. (a) Distribution against the angle $\omega$ of final-state points for the reaction $\pi^- p \to \pi^- \pi^0 p$ at incident lab momentum of 16 GeV/$c$ [3]. (b) The same after correcting for non-constant phase-space effects. The solid lines are the distributions according to the CŁA model [4] normalized to the data after exclusion of the sharp $\rho^-$-resonance. The individual CŁA exchange graphs considered and their contributions to the total distribution are given in sub-figure (c).

Another way of extracting a pure $\Delta$ signal is a separation of the isospin matrix element according to the graph in Fig. 9. Since isospin exchange $I_E = 0$ is excluded for the production of the $I = {}^3/_2$ ($N\pi$)-system, we are left with three matrix elements and their interferences. Their squares, respectively real parts, can readily be extracted model independently from combinations of the 6 measurable (of the 7 possible) final states of $\pi^{\pm}p$ reactions. They are given in Fig. 10 as a function of the ($N\pi$) effective mass. While a wide diffractive shoulder is observed in sub-figure (a), a sharp and well-separated $\Delta$ can be seen in sub-figure (c).
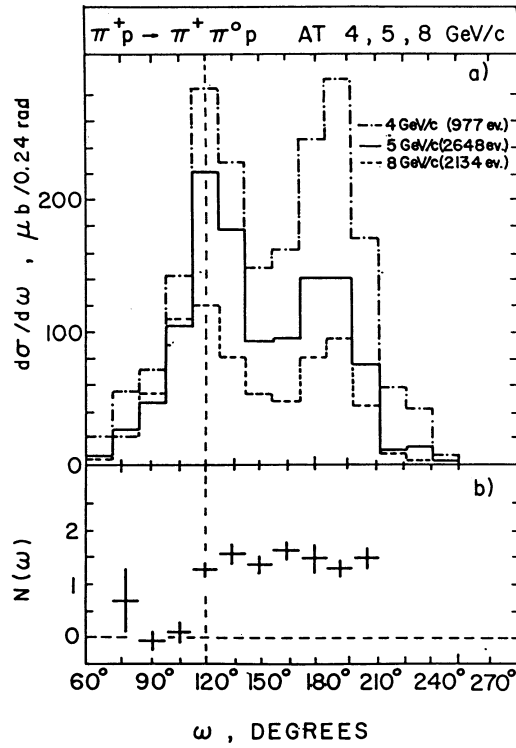
Fig. 5. (a) $\omega$-distribution for the reaction $\pi^+ p \to \pi^+ \pi^0 p$ at incident lab momentum of 4, 5 and 8 GeV/$c$. (b) Exponent $N$ as a function of $\omega$ for the same reaction [5].
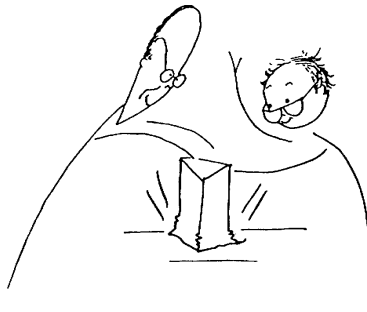


Fig. 6. The prism plot as constructed by pulling a Fabri–Dalitz plot out in the direction of the Van Hove angle $\omega$ (cartoon by Suzy Smile).
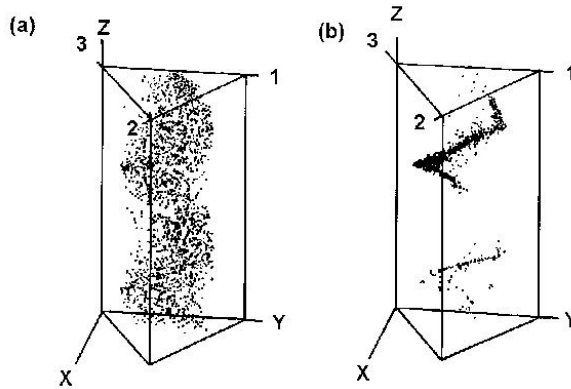
Fig. 7. Prism plot for $\pi^+ p \to \pi^+ \pi^0 p$ at 3.9 GeV/$c$. (a) invariant phase-space and (b) experimental data [6].
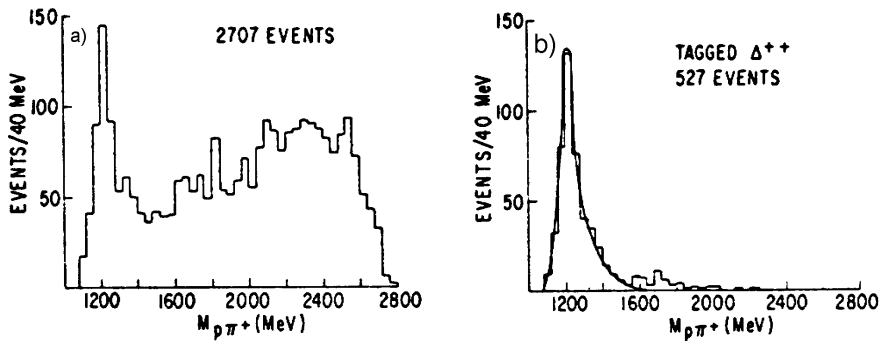


Fig. 8. Effective mass of the $(p\pi^+)$-subsystem for the reaction $\pi^+ p \to \pi^+ \pi^0 p$ at incident lab momentum of 3.9 GeV/$c$, for (a) all events and (b) for events in the corresponding section of the tube in the prism plot [6].



Fig. 9. The three diagrams corresponding to the amplitudes specified by the exchanged isospin $I_E$ and the isospin $I$ of the $(N\pi)$ system. (Note that the combination $I_E = 0, I = \frac{3}{2}$ is excluded from isospin conservation.)

Fig. 10. Squared amplitudes $|M_I^{I_E}|^2$ and their interference terms as functions of the $(N\pi)$ mass obtained from the reactions $\pi^\pm p \to \pi\pi N$ at 16 GeV/$c$ [7].

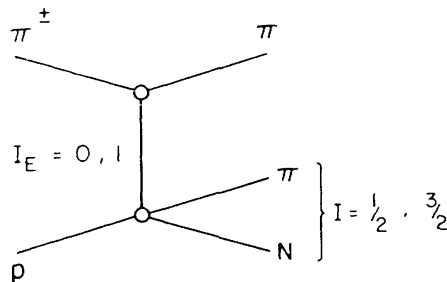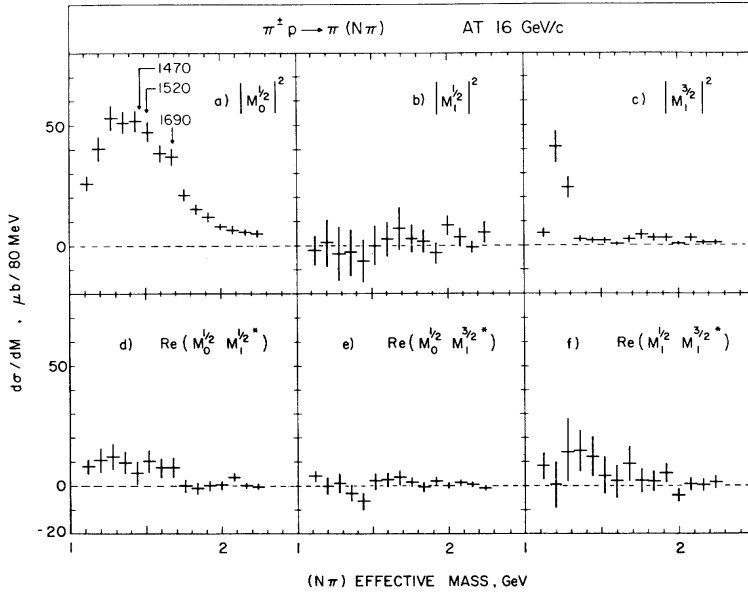Overlap between different sub-systems is a problem, in particular in the determination of spin-parity of a particular sub-system (partial wave analysis). However, interference also provides a unique possibility to study the relative phase between overlapping amplitudes. In such a study, all mechanisms contributing to a particular few-body final state have to be treated simultaneously in an iterative and interactive computer analysis. A beautiful method allowing that is the so-called Analytical Multichannel Analysis [8].

The method has successfully been applied to 30 000 events of the final state of $K^- p \to \bar{K}^0 \pi^- p$ at 4.2 GeV/$c$ [9]. As the four variables needed to describe a three-particle final state, the effective mass $M$ has been used for the sub-system considered, the invariant four-momentum $t'$ in its production and the two angular variables $\Theta$ and $\phi$ of its decay.

As examples for the results after 9 iterations, Figs. 11 and 12 correspond to the $(\bar{K}^0 \pi^-)$ S-wave and its P-waves $J^P M\eta = 1^- 0^-$, $1^- 1^-$ and $1^- 1^+$. Except for the S-wave which is not yet flat, the angular distributions correspond to the particular wave and are as expected. Of particular interest are the differences in the four-momentum $t'$ distributions for the three P-waves, typical for pseudo-scalar and vector exchange, respectively.

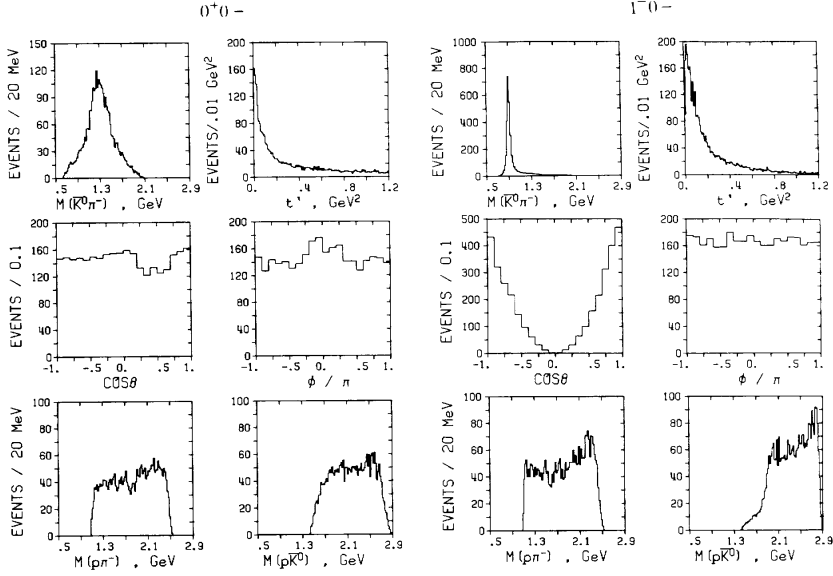Fig. 11. Effective mass distribution of the $(\bar{K}^0\pi^-)$-system, four-momentum transfer $t'$ from initial to final-state proton, decay angles of the $(\bar{K}^0\pi^-)$-system, and effective mass of the $(p\pi^-)$- and $(p\bar{K}^0)$-systems for the $0^+0-$ and $1^-0-$ $(\bar{K}^0\pi^-)$ samples after iteration 9 [9].
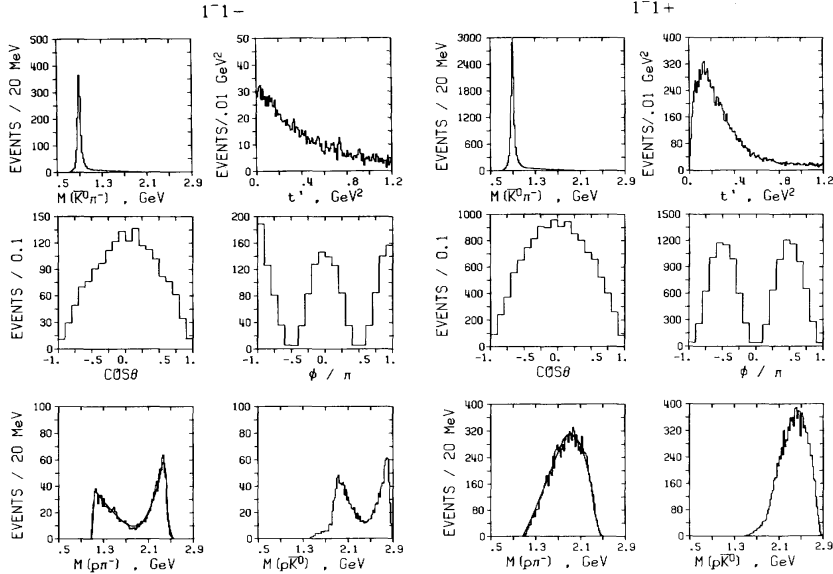


Fig. 12. The same as Fig. 11, but for the $1^-1-$ and $1^-1+$ samples [9].

Striking is the difference in the reflection into the $(p\pi^-)$ and $(p\bar{K}^0)$ systems in the lowest row of Fig. 12. The Monte Carlo curve superimposed on the $(p\pi^-)$ mass distribution shows a two-peak reflection from the $1^-1-$ wave. Just mind the enormous error introduced by the simple smooth hand-drawn background as used in earlier conventional analysis!

Very similar results are obtained [9] for the three D- and even F-waves and for other sub-channels down to the ‰ level of their contribution to the total final state, not detectable in earlier analysis.

In conclusion from this section: With the help of model-independent data analysis, we have moved from analysis in Longitudinal Phase Space to a complete Multichannel Analysis. While the LPS analysis has demonstrated strong correlation of final-state particles, the increased number of variables of the prism plot could show overlap of these mechanisms in full phase space (not just in projections of it). These mechanisms can be separated by means of quantum numbers as isospin, spin and angular momentum, and their interferences can be studied when all channels contributing to a final state are treated simultaneously. This analysis is particularly useful for the isolation of channels at the permille level of cross section or branching ratio.

What had we learned for the future? Experiments have to be *complete* in the sense that acceptance losses should be minimal and the four vectors of all particles should be known. Furthermore, the analysis has to be done *iteratively and interactively, i.e.* has to be guided by computer graphics.

## 2. Momentum correlations and density fluctuations

### 2.1. The formalism

We start by defining symmetrized inclusive $q$-particle distributions

$$\rho_q(p_1, \ldots, p_q) = \frac{1}{\sigma_{\text{tot}}} \frac{\mathrm{d}\sigma_q(p_1, \ldots, p_q)}{\prod_1^q \mathrm{d}p_q}, \tag{6}$$

where $\sigma_q(p_1, \ldots, p_q)$ is the inclusive cross section for $q$ particles to be at $p_1, \ldots, p_q$, irrespective of the presence and location of any further particles, $p_i$ is the (four-) momentum of particle $i$ and $\sigma_{\text{tot}}$ is the total hadronic cross section of the collision under study. For the case of identical particles, integration over an interval $\Omega$ in $p$-space yields

$$\int_\Omega \rho_1(p)\mathrm{d}p = \langle n \rangle, \qquad \int_\Omega \int_\Omega \rho_2(p_1, p_2)\mathrm{d}p_1\mathrm{d}p_2 = \langle n(n-1) \rangle,$$

$$\int_\Omega \mathrm{d}p_1 \ldots \int_\Omega \mathrm{d}p_q \rho_q(p_1, \ldots, p_q) = \langle n(n-1) \ldots (n-q+1) \rangle, \tag{7}$$

where $n$ is the multiplicity of identical particles within $\Omega$ in a given event and the angular brackets imply the average over the event ensemble.

Besides the interparticle *correlations* we are looking for, the inclusive $q$-particle number densities $\rho_q(p_1, \ldots, p_q)$, in general, contain "trivial" contributions from lower-order densities. It is, therefore, advantageous to consider a new sequence of functions $C_q(p_1, \ldots, p_q)$ as those statistical quantities which vanish whenever one of their arguments becomes statistically independent of the others [10–12]

$$C_2(1,2) = \rho_2(1,2) - \rho_1(1)\rho_1(2), \tag{8}$$

$$C_3(1,2,3) = \rho_3(1,2,3) - \sum_{(3)} \rho_1(1)\rho_2(2,3) + 2\rho_1(1)\rho_1(2)\rho_1(3), \tag{9}$$

*etc.* In the above relations, we have abbreviated $C_q(p_1, \ldots, p_q)$ to $C_q(1,2,\ldots,q)$; the summations indicate that all possible permutations must be taken. Expressions for higher orders can be derived from the related formulae given in [13]. Deviations of these functions from zero shall be addressed as *genuine* correlations.

It is often convenient to divide the functions $\rho_q$ and $C_q$ by the product of $q$ one-particle densities, which leads to the definition of the normalized inclusive densities and correlations

$$R_q(p_1, \ldots, p_q) = \rho_q(p_q, \ldots, p_q)/\rho_1(p_1) \ldots \rho_1(p_q), \tag{10}$$

$$K_q(p_1, \ldots, p_q) = C_q(p_1, \ldots, p_q)/\rho_1(p_1) \ldots \rho_1(p_q). \tag{11}$$

In terms of these functions, correlations have been studied extensively for $q = 2$. Results also exist for $q = 3$, but usually the statistics (*i.e.* number of events available for analysis) are too small to isolate genuine correlations. To be able to do that for $q \geq 3$, one must apply factorial moments $F_q$ defined via the integrals Eq. (7), but in limited phase-space cells [14–16].

### 2.2. Density spikes

To see whether it is worth the effort, we first look for density fluctuations in single events, signalling high-order correlations. A notorious JACEE event [17] (Fig. 13 (a)) at a pseudo-rapidity resolution (binning) of $\delta\eta = 0.1$ has local fluctuations up to $\mathrm{d}n/\mathrm{d}\eta \approx 300$ with a signal-to-background ratio of about 1:1. An NA22 event [18] (Fig. 13 (b)) contains a "spike" at a rapidity resolution $\delta y = 0.1$ of $\mathrm{d}n/\mathrm{d}y = 100$, as much as 60 times the average density in this experiment.
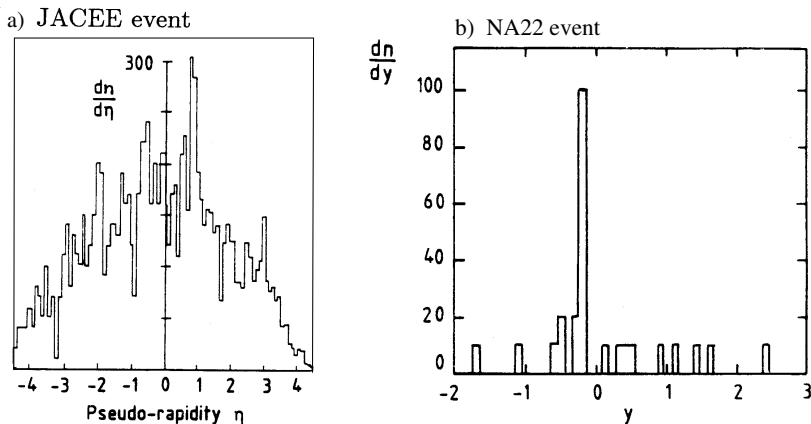
Fig. 13. (a) The JACEE event [17]; (b) The NA22 event [18].

Bialas and Peschanski [14, 15] suggested that this type of spikes could be a manifestation of "intermittency", a phenomenon well-known in fluid dynamics [19]. The authors argued that if intermittency indeed occurs in particle production, large density fluctuations are not only expected, but should also exhibit self-similarity with respect to the size of the phase-space volume.

In multiparticle experiments, the number of hadrons produced in a single collision is small and subject to considerable noise. To exploit the techniques employed in complex-system theory, a method had to be devised to separate fluctuations of purely statistical (Poisson) origin, due to finite particle numbers, from possibly self-similar dynamical fluctuations of the underlying particle densities. A solution, already used in quantum optics [20] and suggested for multiparticle production in [14], consists in measuring $F_q(\delta y)$ in given phase-space volumes (resolution) $\delta y$ of ever decreasing size.

### 2.3. Power-law scaling

Besides the property of noise-suppression, high-order factorial moments act as a filter and resolve the large-multiplicity tail of the multiplicity distribution. They are thus particularly sensitive to large density fluctuations at the various scales $\delta y$ used in the analysis. As shown in [14], a smooth density distribution, which does not show any fluctuations except for the statistical ones, has the property of normalized factorial moments $F_q(\delta y)$ being independent of the resolution $\delta y$ in the limit $\delta y \to 0$. On the other hand, if self-similar dynamical fluctuations exist, the $F_q$ obey the power law

$$F_q(\delta y) \propto (\delta y)^{-\phi_q}, \qquad (\delta y \to 0). \tag{12}$$

Equation (12) is a scaling law since the ratio of the factorial moments at resolutions $L$ and $\ell$

$$R = \frac{F_q(\ell)}{F_q(L)} = \left(\frac{L}{\ell}\right)^{\phi_q} \tag{13}$$

only depends on the ratio $L/\ell$, but not on $L$ and $\ell$ themselves.

In Fig. 14, $\log F_5$ is plotted [14] as a function of $-\log \delta\eta$ ($\eta$ is the pseudorapidity) for the JACEE event. It is compared with an independent-emission Monte Carlo model tuned to reproduce the average $\eta$ distribution of Fig. 13 (a) and the global multiplicity distribution, but has no short-range correlations. While the Monte Carlo model indeed predicts constant $F_5$, the JACEE event shows a first indication for a linear increase, *i.e.* a possible sign of intermittency.
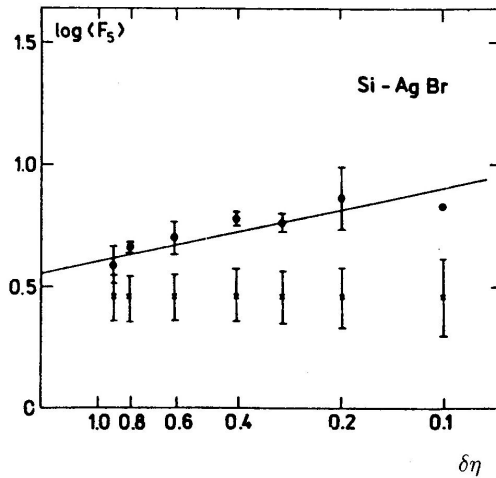


Fig. 14.   $\log F_5$ as a function of $-\log \delta\eta$ for the JACEE event [17] (full circles) compared to independent emission (small crosses) [14].

This observation was the trigger for a tremendous outburst of experimental research on all types of collisions from $e^+e^-$ to heavy nuclei, all showing (approximate) power-law scaling. An 118 page summary including more than 300 references is given as chapters 7 and 10 in [21].

The powers $\phi_q$ (slopes in a double-log plot) are related [22] to the anomalous (or co-) dimensions $d_q = \phi_q/(q-1)$, a measure for the deviation from an integer dimension.

Anomalous dimensions $d_q$ fitted over the (one-dimensional) range of $0.1 < \delta y < 1.0$ are compiled in Fig. 15 [23]. They typically range from $d_q = 0.01$ to $0.1$, which means that the fractal (Rényi) dimensions $D_q = 1 - d_q$ are close to

one. The $d_q$ are larger and grow faster with increasing order $q$ in $\mu p$ and $e^+e^-$ (Fig. 15 (a)) than in $hh$ collisions (Fig. 15 (b)), and are small and almost independent of $q$ in heavy-ion collisions (Fig. 15 (c)). For $hh$ collisions, the $q$-dependence is considerably stronger for NA22 ($\sqrt{s} = 22$ GeV, all $p_T$) than for UA1 ($\sqrt{s} = 630$ GeV, $p_T > 0.15$ GeV/$c$).
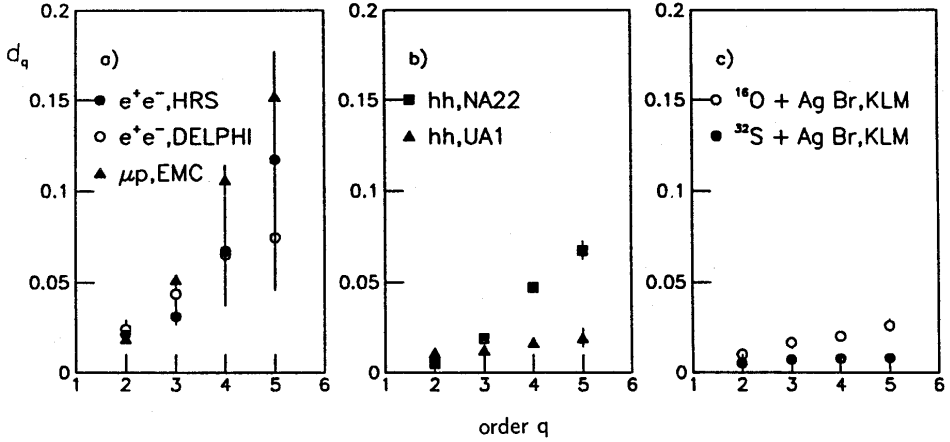


Fig. 15. Anomalous dimension $d_q$ as a function of the order of $q$, for (a) $\mu p$ and $e^+e^-$ collisions, (b) NA22 and UA1, (c) KLM [23].

## 2.4. Factorial cumulants

One further has to stress the advantages of normalized factorial cumulants $K_q$ compared to factorial moments, since the former measure *genuine* correlation patterns.

As an example, high statistics data of the OPAL experiment [24] are given in Fig. 16 in terms of $K_q$, as a function of the number $M \propto 1/\delta y$ of phase-space partitions for $q = 3$ to 5. In the leftmost column, the one-dimensional rapidity variable $y$ is used for the analysis. The data (black dots) show an increase of $K_q$ with increasing $M$ for small $M$, but a saturation at larger $M$. Even though weaker, some saturation still persists when the analysis is done in the two-dimensional plane of rapidity $y$ and azimuthal angle $\varphi$ (middle column), but approximate power-law scaling is indeed observed for the analysis in three-dimensional momentum space (right column). Thus, in high-energy collisions, fractal behaviour is fully developed in three dimensions, while projection effects lead to saturation in lower dimension.

In Fig. 16, the data are also compared to a number of parametrizations of the multiplicity distributions, as well as to the Monte Carlo models JET-SET and HERWIG. One can see that the fluctuations given by the negative
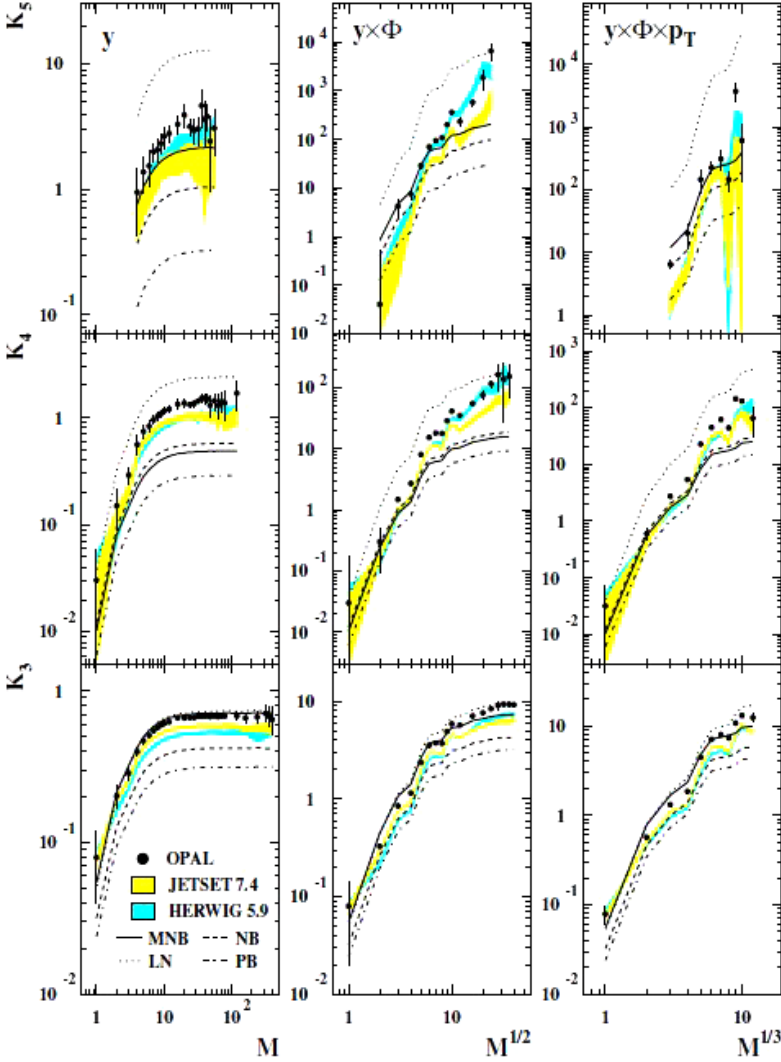
Fig. 16. Cumulants of the order of $q = 3$ to $5$ as a function of $M^{1/D}$ in comparison with the predictions of various multiplicity parametrizations and two Monte Carlo models [24].

binomial (NB) (dashed line) are weaker than observed in the data. Contrary to the NB, the log-normal (LN) distribution (dotted line) overestimates the cumulants, while these expected for a pure birth (PB) process (dash-dotted) underestimate the data even more significantly than the NB. Among the distributions shown, a modified NB (MNB) gives the best results, even though significant underestimation is observed also there. The Monte Carlo models do surprisingly well.

### 2.5. *Transverse-momentum dependence*

An interesting question is whether semi-hard effects [25], observed to play a role in the transverse-momentum behaviour even at NA22 energies [26], or low-$p_T$ effects [27, 28] are at the origin of intermittency. A first indication for the latter comes from the most prominent NA22 spike event (Fig. 13 (b)), where 5 out of 10 tracks in the spike have $p_T < 0.15$ GeV/$c$.

In Fig. 17, NA22 data [29] on $\ln F_q$ *versus* $-\ln \delta y$ are given for particles with transverse momentum $p_T$ below and above 0.15 GeV/$c$, and with $p_T$ below and above 0.3 GeV/$c$. For particles with $p_T$ below the cut (left), the $F_q$ exhibits a far stronger $\delta y$ dependence than for particles with $p_T$ above the cut (right).
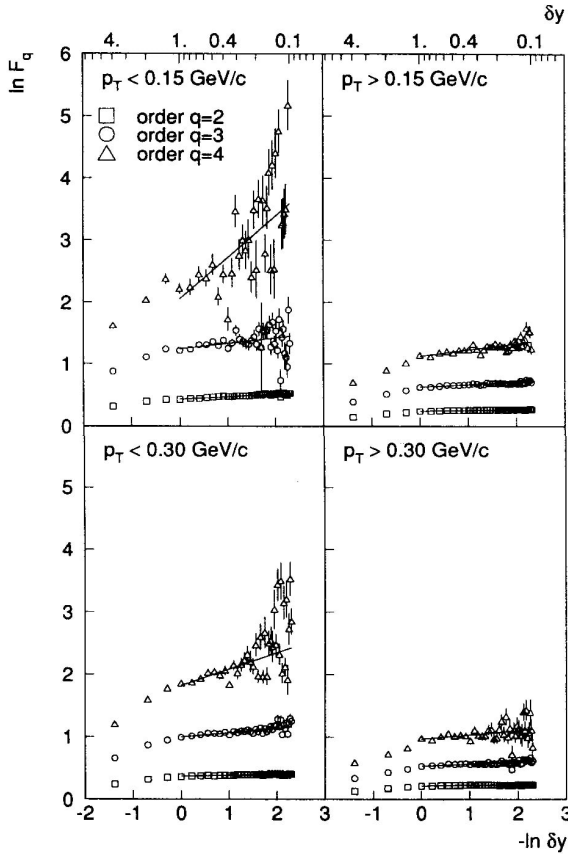


Fig. 17. $\ln F_q$ as a function of $-\ln \delta y$ for various $p_T$ cuts as indicated [29].

UA1 has a bias against $p_T < 0.15$ GeV/$c$ and the anomalous dimension is indeed smaller in UA1 than in NA22 in Fig. 15. We conclude that intermittency in $hh$ collisions is not dominated by semi-hard effects.

## 2.6. Energy and multiplicity dependence

As seen in Fig. 18, a strong multiplicity dependence of the intermittency strength is observed for *hh* collisions by UA1 [30]. The trend is opposite to the predictions of the models used by this collaboration. This decrease of the intermittency strength with increasing multiplicity is usually explained as a consequence of mixing of independent sources of particles [22].



Fig. 18. (a) Multiplicity dependence of the slope $\phi_3$, compared to that expected from a number of models, the crosses correspond to a combination of independent events [30], (b) slope $\phi_2$ extrapolated ($\propto \rho^{-1}$) as a function of particle density from NA22 (*hp* at 250 GeV) (solid line) and heavy-ion collisions as indicated [33].

Mixing of emission sources leads to a roughly linear decrease of the slopes $\phi_q$ with increasing particle density $\langle\rho\rangle$ in rapidity [15, 31, 32]: $\phi_q \propto \langle\rho\rangle^{-1}$. This is indeed observed by UA1 [30].

Figure 18 (a) helps in explaining why intermittency is so weak in heavy-ion collisions (*cf.* Fig. 15): the density (and mixing of sources) is particularly high there. In Fig. 18 (b), EMU01 [33], therefore, compares $\phi_2$ for NA22 (*hp* at 250 GeV) and heavy-ion collisions at similar beam momentum per nucleon, as a function of the particle density. Whereas slopes averaged over multiplicity are smaller for *AA* collisions than for NA22 in Fig. 15, at fixed $\langle\rho\rangle$ they are actually higher than expected from an extrapolation of *hh* collisions to high density and may even grow with increasing size of the nuclei. The trend is confirmed by KLMM [34] for intermittency in azimuthal angle $\varphi$ and for slopes up to the order of 5. This may be evidence

for re-scattering (see [35]) or another (collective) effect, but, as shown by
HELIOS [36] and confirmed by EMU-01 [33], one has to be very sure about
the exclusion of $\gamma$-conversions before drawing definite conclusions.

### 2.7. Density and correlation integrals

A fruitful development in the study of density fluctuations is the density
and correlation strip-integral method [37] illustrated in Fig. 19 [38]. By
means of integrals of the inclusive density over a strip domain in $y_1, y_2$
space, rather than a sum of box domains, one not only avoids unwanted
side-effects such as splitting of density spikes, but also drastically increases
the integration volume (and therefore the statistical significance) at given
resolution. In terms of the strips (or hyper-tubes for $q > 2$), the density
integrals can be evaluated directly from the data after selection of a proper
distance measure, as *e.g.* the four-momentum difference $Q_{ij}^2 = -(p_i - p_j)^2$,
and after definition of a proper multiparticle topology (snake integral [39],
GHP integral [37], star integral [40]). Similarly, *correlation* integrals can
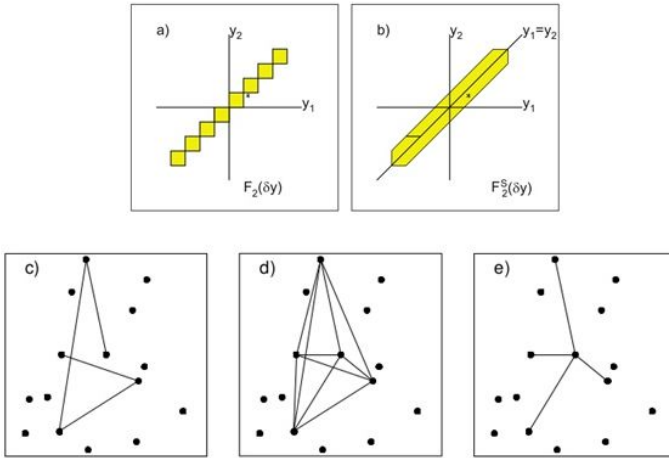be defined by replacing the density $\rho_q$ in the integral by the correlation
function $C_q$.



Fig. 19. (a) The integration domain $\Omega_{\mathrm{B}} = \Sigma_m \Omega_m$ of $\rho_2(y_1, y_2)$ for the bin-averaged
factorial moments, (b) the corresponding integration domain $\Omega_{\mathrm{S}}$ for the density
integral, (c) illustration of a $q$-tuple in snake topology, (d) GHP topology, (e) star
topology [38].

Of particular interest is a comparison of hadron–hadron to $e^+e^-$ results
in terms of the same and opposite charges of the particles involved. Such
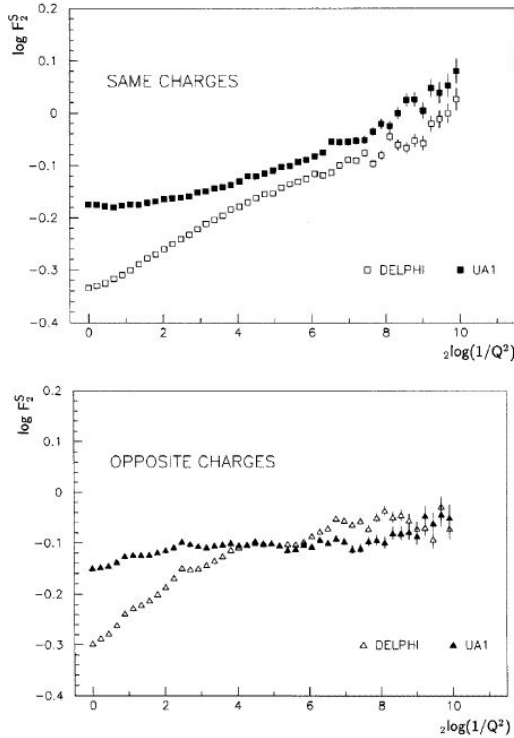a comparison is shown in Fig. 20 for $q = 2$ [41]. An important difference

Fig. 20. Comparison of density integrals for $q = 2$ in their differential form (in intervals $Q^2, Q^2 + \mathrm{d}Q^2$) as a function of $_2 \log(1/Q^2)$ for $e^+ e^-$ (DELPHI) and hadron–hadron collisions (UA1) [41].

between UA1 and DELPHI can be observed in comparison of the two subfigures: For relatively large $Q^2 (> 0.03 \; \mathrm{GeV}^2)$, where Bose–Einstein effects do not play a major role, the $e^+ e^-$ data increase much faster with increasing $-_2 \log Q^2$ than the hadron–hadron results. For $e^+ e^-$, the increase in this $Q^2$ region is very similar for the same and for opposite-sign charges. At small $Q^2$, however, the $e^+ e^-$ results approach the $hh$ results. For $e^+ e^-$ annihilation at LEP, at least two processes are considered to be responsible for the power-law behaviour: Bose–Einstein correlation at small $Q^2$ following the evolution of jets at larger $Q^2$, but what is remarkable is the smooth transition between the two domains (if at all present) (see Sect. 3).

## 2.8. Genuine higher-order correlations

The correlation integral method turns out particularly useful for the unambiguous establishment of genuine higher-order correlations in terms of the normalized cumulants $K_q(Q^2)$, when using the star integration [40].

Non-zero values of (star integral) $K_q^*(Q^2)$ increasing according to a power law with decreasing $Q^2$ were first observed in NA22 up to the fifth order [42] (see Fig. 21) and in E665 for the third order [43]. Again, note the difference between all charged and like-charged particles, and the smooth transition between larger and smaller $Q^2$.
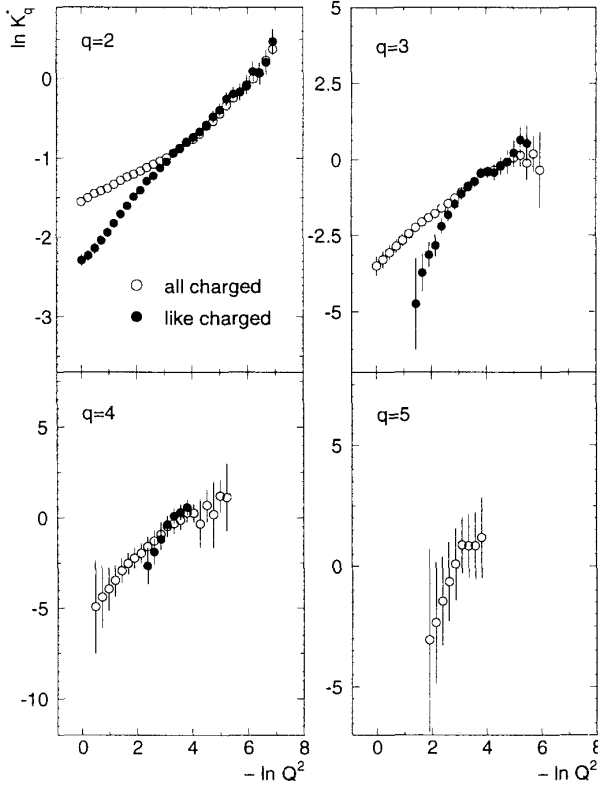


Fig. 21. $\ln K_q^*(Q^2)$ as a function of $-\ln Q^2$ for all charged particles as well as for like-charged particles [42].

## 2.9. Functional form

The exact functional form of $F_2^S$ is derived from the data of UA1 [30] and NA22 [38][1] in Fig. 22. Clearly, the data favour a power law in $Q$ over an exponential, double-exponential or Gaussian law.

If the observed effect is real, it supports a view developed in [44]. There, intermittency is explained from Bose–Einstein correlations between (like-charged) pions. As such, Bose–Einstein correlations from a static source are

---

[1] In fact, in this form, $F_2^S(Q^2)$ is identical to $R(Q^2)$ usually used in Bose–Einstein analysis. The only difference is that here it is plotted on a double-logarithmic plot.
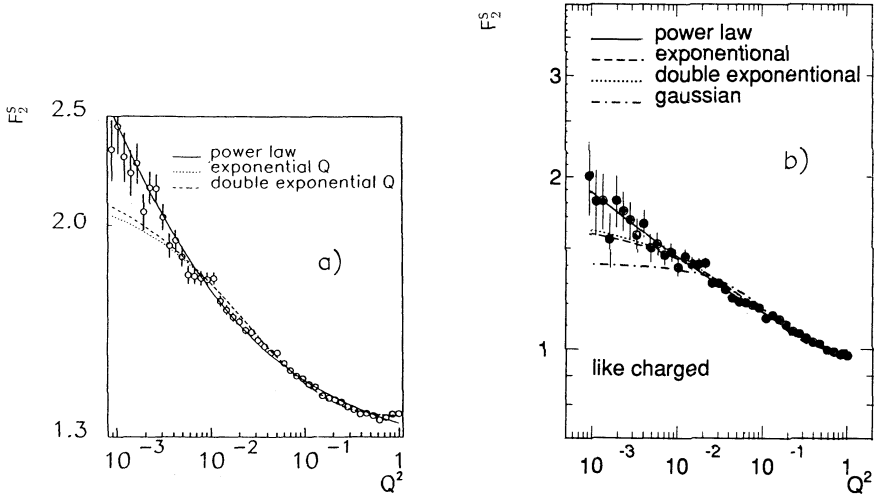
Fig. 22. Density integrals $F_2^{\mathrm{S}}$ (in their differential form) as a function of $Q^2$ for like-charged pairs in UA1 [30] and NA22 [38], compared to power-law, exponential, double-exponential and Gaussian fits, as indicated.

not power behaved. A power law is obtained *(i)* if the size of the interaction region is allowed to fluctuate, and/or *(ii)* if the interaction region itself is assumed to be a self-similar object extending over a large volume. Condition *(ii)* would be realized if parton avalanches were to arrange themselves into self-organized critical states [45]. Though quite speculative at this moment, it is an interesting new idea with possibly far-reaching implications. We should mention also that in such a scheme, intermittency is viewed as a final-state effect and is, therefore, not troubled by hadronization effects.

So, in conclusion of this section, (approximate) intermittency is found to be all-present in hadron production and is evidence for genuine correlations to high orders, but it seems dominated by Bose–Einstein correlations. However, what we have learned is that we have been fooled for more than half a century by an assumed Gaussian behaviour of the BE correlations, while an approximate power law is required. This highly non-trivial lesson we have learned indeed sheds a completely new light on the topic of femtoscopy.

## 3. Bose–Einstein correlations (or what?)

### 3.1. Early results

Whether derived as Fourier transform of a (static and chaotic) pion source distribution, a covariant Wigner-transform of the (momentum dependent) source density matrix, or from the string model, identical-pion

correlation leads to a positive, non-zero two-particle correlator $K_2(Q)$, *i.e.* to

$$R_2(Q) = 1 + K_2(Q) > 1 \qquad (14)$$

at small four-momentum difference $Q$. These so-called Bose–Einstein correlations, by now, are a well-established effect in all types of collisions, even in hadronic $Z^0$ decay (for reviews, see [21, 46, 47]) originally expected, however, to be too coherent to show an effect.

Other important observations are given in abstract form below.

1. When evaluated in two (or better three) dimensions in the Bertsch–Pratt system, a small elongation of the emission region (better region) of homogeneity [48] is observed along the event axis in all types of collisions (hadron–hadron [49], all four LEP experiments [50], ZEUS [51], RHIC [52]). However, it is important to note that the longitudinal radius of homogeneity is much shorter than the length of the sting (of the order of 1%).

   The observation that the out-radius does not grow beyond the side-radius at RHIC [52] points to a short duration of emission and causes a problem for some hydrodynamical models, but not for *e.g.* the Buda–Lund hydro model. The latter, in fact, gives a beautifully consistent description of single-particle spectra and BEC in hadron–hadron and heavy-ion collisions at SPS and RHIC [53]. The emission function resembles a Gaussian shaped fire-ball for $AA$ collisions, but a fire-tube for $hh$ collisions.

2. The form of the correlator at small $Q$ is steeper than Gaussian, in fact, consistent with a power law as would be expected from the intermittency phenomenon described above. Unifying progress is reported in [54].

3. An approximate $m_{\mathrm{T}}^{-1/2}$ scaling first observed in heavy-ion collisions at the SPS [55] and usually blamed on collective flow, is observed at RHIC [56], but also in $e^+e^-$ collisions [57]. Quite generally, it follows from a strong position momentum correlation [58, 59], be it due to collective flow or to string fragmentation.

4. *Genuine three-pion correlations* exist in all types of collisions and, in principle, allow a phase to be extracted from

$$\cos\phi \equiv \omega(Q_3) = K_3(Q_3)/2\sqrt{K_2(Q_3)}. \qquad (15)$$

   At small $Q$, this $\omega$ is near unity (as expected from incoherence) for $hh$ [60] and $e^+e^-$ [61] collisions, as well as for PbPb [62, 63] and

AuAu [64] collisions at SPS and RHIC, while it is near zero (compatible with full coherence) in collisions of light nuclei [62]. This contradiction can be solved [46, 65] if $\omega$ is interpreted as a ratio of normalized cumulants. Since $K_q^{(N)}$ of $N$-independent overlapping sources gets diluted like $1/N^{q-1}$, $\omega$ would be reduced if strings produced by light ions do not interact. If, in *heavy*-ion collisions, the string density gets high enough for them to coalesce, some kind of percolation sets in and full inter-string BEC gets restored.

5. Azimuthal anisotropy is observed in configuration space of non-central heavy-ion collisions at AGS energies [66], but also at RHIC [67]. Contrary to elliptic flow, it is directed out of the event plane, but consistent with the elliptic nuclear overlap in a non-central collision. Due to larger pressure in the event plane, the anisotropy gets reduced but not destroyed at RHIC. Also this is evidence for a short duration of pion emission.

### 3.2. The $\tau$ model

In $e^+e^-$, BEC depend, at least approximately, only on $Q$ and not on its components separately, in the sense that $e^+e^-$ BEC is large if $Q$ is small even when any of its components are large. Further, $R_2$ shows anti-correlations in the region of 0.6–1.5 GeV as observed by L3 at LEP [68] as well as by CMS [69] and ATLAS (preliminary) [70] at the LHC (see Fig. 23).

A model which predicts such $Q$-dependence, as well as the absence of dependence on the components of $Q$ separately, is the so-called $\tau$ model [58]. Further, it incorporates the Bjorken–Gottfried condition [59, 71] whereby the four-momentum of a produced particle and the space-time position at which it is produced are linearly related.

In this model, it is assumed that the average production point in the overall center-of-mass system, $\overline{x} = (\overline{t}, \overline{r}_x, \overline{r}_y, \overline{r}_z)$, of particles with a given four-momentum $p = (E, p_x, p_y, p_z)$ is given by

$$\overline{x}^{\mu}(p^{\mu}) = a\tau p^{\mu} \,. \tag{16}$$

In the case of two-jet events, $a = 1/m_{\mathrm{T}}$, where $m_{\mathrm{T}}$ is the transverse mass and $\tau = \sqrt{\overline{t}^2 - \overline{r}_{\mathrm{z}}^2}$ is the longitudinal proper time. For isotropically distributed particle production, the transverse mass is replaced by the mass in the definition of $a$ and $\tau$ is the proper time, $\sqrt{\overline{t}^2 - \overline{r}_x^2 - \overline{r}_y^2 - \overline{r}_z^2}$.

The second assumption is that the distribution of $x^{\mu}(p^{\mu})$ about its average, $\delta_{\Delta}(x^{\mu}(p^{\mu}) - \overline{x}^{\mu}(p^{\mu}))$, is narrower than the proper-time distribution, $H(\tau)$. Then, the two-particle Bose–Einstein correlation function is, indeed, found
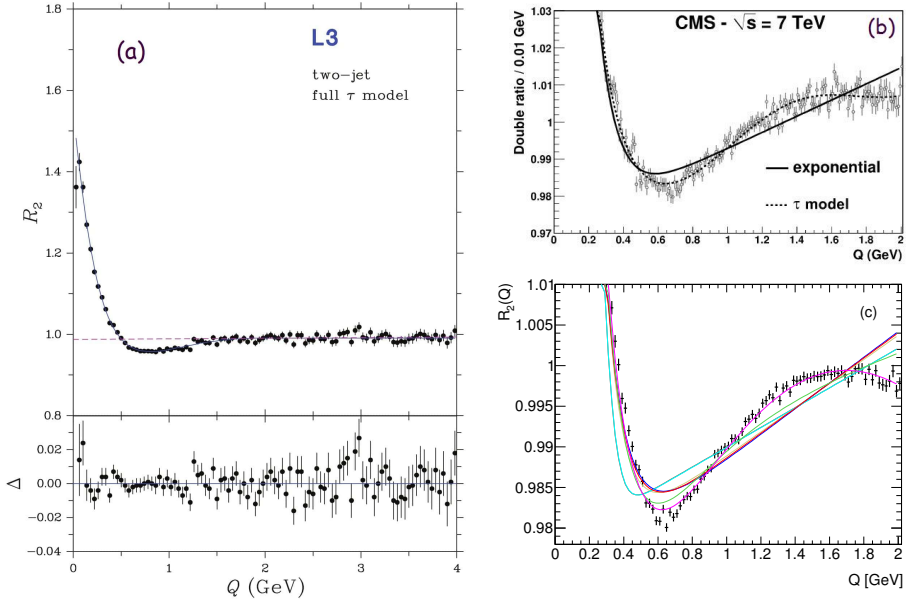
Fig. 23. The Bose–Einstein correlation function $R_2$ for (a) L3 [68], (b) CMS [69] and (c) ATLAS [70]. The curve in (a), the dashed line in (b) and the best fit in (c) correspond to the fit of the $\tau$ model. The results of the L3 fit are given in Table I. Also plotted in (a) is $\Delta$, the difference between the fit and the data. The dashed line represents the long-range part of the fit, i.e., $\gamma(1 + \epsilon Q)$. The solid line in (b) is an exponential fit. The lines in (c) correspond to Gaussian, exponential, and $\tau$ model fits.

to depend on the invariant relative momentum $Q$, rather than on its separate components, as well as on the values of $a$ of the two particles [72]:

$$R_2(p_1, p_2) = 1 + \mathrm{Re}\widetilde{H}\left(\frac{a_1 Q^2}{2}\right)\widetilde{H}\left(\frac{a_2 Q^2}{2}\right), \qquad (17)$$

where $\widetilde{H}(\omega) = \int \mathrm{d}\tau H(\tau)\exp(i\omega\tau)$ is the Fourier transform (characteristic function) of $H(\tau)$. (Note that $H(\tau)$ is normalized to unity.)

Since there is no particle production before the onset of the collision, $H(\tau)$ should be a one-sided distribution. In the leading log approximation of QCD, the parton shower is a fractal [73]. Further, a Lévy distribution arises naturally from a fractal [74]. One is thus led to choose a one-sided Lévy distribution for $H(\tau)$ [72]. The characteristic function of $H(\tau)$ can then be written [75] (for $\alpha \neq 1$) as

$$\widetilde{H}(\omega) = \exp\left[-\frac{1}{2}\left(\Delta\tau|\omega|\right)^{\alpha}\left(1 - i\,\mathrm{sign}(\omega)\tan\left(\frac{\alpha\pi}{2}\right)\right) + i\,\omega\tau_0\right], \qquad (18)$$

where the parameter $\tau_0$ is the proper time of the onset of particle production and $\Delta\tau$ is a measure of the width of the proper-time distribution. $0 < \alpha < 2$ is the so-called index of stability [76] of the Lévy distribution. Using this characteristic function in (17), and incorporating the usual strength factor $\lambda$ and the long-range parametrization, yields

$$R_2(Q, a_1, a_2) = \gamma\left\{1 + \lambda\cos\left[\frac{\tau_0 Q^2(a_1+a_2)}{2} + \tan\left(\frac{\alpha\pi}{2}\right)\left(\frac{\Delta\tau Q^2}{2}\right)^{\alpha}\frac{a_1^{\alpha}+a_2^{\alpha}}{2}\right]\right.$$

$$\left. \times \exp\left[-\left(\frac{\Delta\tau Q^2}{2}\right)^{\alpha}\frac{a_1^{\alpha}+a_2^{\alpha}}{2}\right]\right\}(1+\epsilon Q). \qquad (19)$$

It is the cosine factor which generates oscillations corresponding to alternating correlated and anti-correlated regions mentioned above. Note also that since $a = 1/m_T$ for two-jet events, the $\tau$ model predicts a decrease of the effective source size with increasing $m_T$.

For each bin in $Q$, the average values of $m_{T1}$ and $m_{T2}$ are calculated, where $m_{T1}$ and $m_{T2}$ are the transverse masses of the two particles making up a pair, requiring $m_{T1} > m_{T2}$. Using these averages, (19) is fit to $R_2(Q)$ by the L3 Collaboration [68]. The fit results in $\tau_0 = 0.00 \pm 0.02$ fm, and the results of a re-fit with $\tau_0$ fixed to zero are shown in Table I.

TABLE I

Results of the fit of (19) for two-jet events, as shown in Fig. 23 (a) [68]. The parameter $\tau_0$ is fixed to zero. The first uncertainty is statistical, the second systematic.

| Parameter | |
|---|---|
| $\lambda$ | $0.58 \pm 0.03^{+0.08}_{-0.24}$ |
| $\alpha$ | $0.47 \pm 0.01^{+0.04}_{-0.02}$ |
| $\Delta\tau$ [fm] | $1.56 \pm 0.12^{+0.32}_{-0.45}$ |
| $\epsilon$ [GeV$^{-2}$] | $0.001 \pm 0.001 \pm 0.003$ |
| $\gamma$ | $0.988 \pm 0.002^{+0.006}_{-0.002}$ |
| $\chi^2$/d.o.f. | $90/95$ |
| C.L. | $62\%$ |

Note that no significant long-range correlation is observed: $\epsilon = 0$ well within one standard deviation and $\gamma$ is close to unity. Obviously, the $\tau$ model by itself can reproduce the (smooth) shape of the $Q$-distribution over the full range considered, the anticorrelation near $Q = 0.6$ GeV included.

In the $\tau$ model, the basic assumption is the Bjorken–Gottfried condition [59, 71] leading to (16). Recently, it has been demonstrated by the same authors [77], however, that already the compositeness of pions can most naturally lead to an anti-correlation. At small distances, the constituents mix and there are no separate pions to interfere.

### 3.3. The emission function

The $\tau$ model results for BEC can be used together with the single-particle inclusive spectra to reconstruct the space-time evolution of hadronization. The emission function in configuration space, $S_x(x)$, is the proper time derivative of the integral over $p$ of $S(x, p)$ [72]. Approximating $\delta_\Delta$ by a Dirac delta function again, gives

$$S_x(x) = \frac{1}{\bar{n}} \frac{\mathrm{d}^4 n}{\mathrm{d}\tau \mathrm{d}^3 x} = \left(\frac{m_\mathrm{T}}{\tau}\right)^3 H(\tau) \rho_1\left(p = \frac{m_\mathrm{T} x}{\tau}\right), \qquad (20)$$

where $n$ and $\bar{n}$ are the number and average number of pions produced, respectively, and $\rho_1(p)$ is the experimentally measurable single-particle spectrum.

Given the symmetry of two-jet events, $S_x$ does not depend on the azimuthal angle, and one can write it in cylindrical coordinates as

$$S_x(r, z, t) = P(r, \eta) H(\tau), \qquad (21)$$

where $\eta$ is the space-time rapidity. With the strongly correlated phase space of the $\tau$ model, $\eta$ is equal to the momentum-energy rapidity $y$ and $r = p_\mathrm{T} \tau / m_\mathrm{T}$. Consequently,

$$P(r, \eta) = \left(\frac{m_\mathrm{T}}{\tau}\right)^3 \rho_{p_\mathrm{T}, y}(r m_\mathrm{T}/\tau, \eta), \qquad (22)$$

where $\rho_{p_\mathrm{T}, y}$ is the joint single-particle distribution of $p_\mathrm{T}$ and $y$.

The reconstruction of $S_x$ is simplified if $\rho_{p_\mathrm{T}, y}$ can be factorized into the product of the single-particle $p_\mathrm{T}$ and rapidity distributions, i.e., $\rho_{p_\mathrm{T}, y} = \rho_{p_\mathrm{T}}(p_\mathrm{T}) \rho_y(y)$. Then, (22) becomes

$$P(r, \eta) = \left(\frac{m_\mathrm{T}}{\tau}\right)^3 \rho_{p_\mathrm{T}}(r m_\mathrm{T}/\tau) \rho_y(\eta). \qquad (23)$$

The integral over the transverse distribution is shown in Fig. 24. It exhibits a "boomerang" shape with a maximum at low $t$ and $z$, but with tails reaching out to very large values of $t$ and $z$, a feature already observed for hadron–hadron [78, 79] and heavy-ion collisions [80] (Fig. 25 (a) and (c)) in the framework of a hydrodynamical model [81].
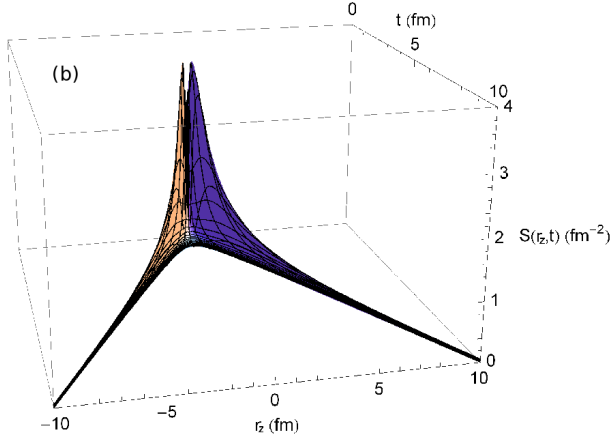
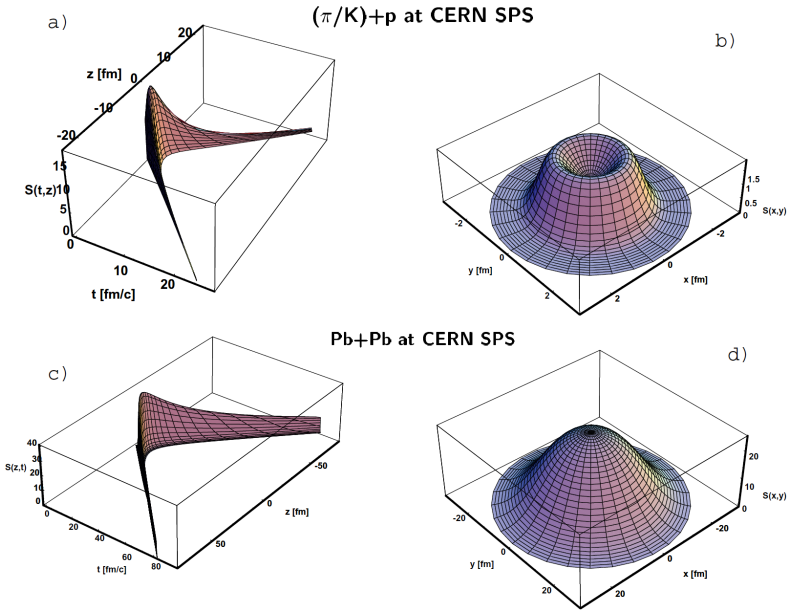Fig. 24. The temporal-longitudinal part of the emission function normalized to unity [68].



Fig. 25. The reconstructed emission function $S(t, z)$ in arbitrary vertical units, as a function of time $t$ and longitudinal coordinate $z$ (left diagrams), as well as the reconstructed emission function $S(x, y)$ in arbitrary vertical units, as a function of the transverse coordinates $x$ and $y$ (right pictures), for $hh$ (upper pictures) and PbPb (lower pictures) collisions, respectively [78–80].

The transverse part of the emission function is obtained by integrating over $z$ as well as azimuthal angle. Figure 26 shows the transverse part of the emission function for various proper times. Particle production starts immediately, increases rapidly and decreases slowly. In the transverse direction, a ring-like structure is observed similar to the expanding, ring-like wave created by a pebble in a pond. This ring-like structure was also observed in hadron–hadron collisions [78] (Fig. 25 (b)), where it was interpreted as due to the production of a fire-ring. Despite this similarity, the physical process is different. Reflecting a non-thermal nature of $e^+e^-$ annihilation, the proper-time distribution and space-time structure are reconstructed here without any reference to a temperature.
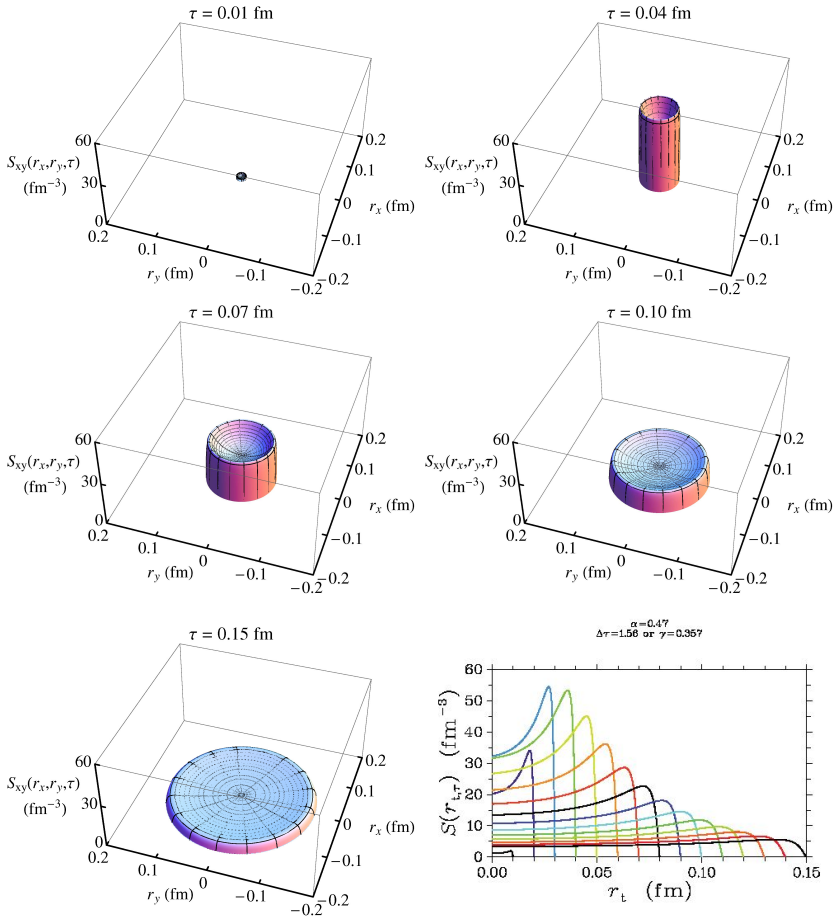


Fig. 26. The transverse emission function normalized to unity, and its transverse profile for various proper times [68]. An animated gif file covering the first $0.15\,\mathrm{fm} = 0.5 \times 10^{-24}$ sec is available [82].

Interpolating and extrapolating Fig. 26, the proper-time dependence of the transverse expansion of the emission function can be best shown in a movie that ends in 0.15 fm ($0.5 \times 10^{-24}$ sec), making it the shortest movie ever made of a process in nature [82].

In conclusion, I find it absolutely amazing how the combination of experimental results on single particle spectra and two-particle correlations with some theoretical interpretation can allow us to construct a "femtoscope" and actually watch particle production at a scale below one fm taking place in less than $10^{-24}$ sec!

However, one basic puzzle remains: why in the world should pions thought to be produced *coherently* in a flux tube (at least in $e^+e^-$ and TeV $pp$ collisions) be subject to *incoherent* Bose–Einstein correlations? Have we fooled ourselves for the past half century or more? Perhaps! What Todorova-Nová is trying to tell us in a series of papers [83] based on the Lund Helix model [84] is just that. Bose–Einstein correlations may not be needed to explain the charge asymmetry of pion pair production, a helix shaped flux tube would not only generate transverse momenta and hadronic masses, but a sharp correlation peak for like-charged pion pairs at low values of four-momentum difference $Q$. I think, it should be a fruitful challenge for younger ones among us to help sort that out in detail in the future.

## REFERENCES

[1] L. Van Hove, *Phys. Lett. B* **28**, 429 (1969); *Nucl. Phys. B* **9**, 331 (1969).

[2] A. Bialas, A. Eskreys, W. Kittel, S. Pokorski, J.K. Tuominiemi, L. Van Hove, *Nucl. Phys. B* **11**, 479 (1969).

[3] J. Bertsch *et al.* [ABBCHLV Coll.], *Nucl. Phys. B* **19**, 381 (1970).

[4] Chan Hong-Mo, J. Łoskiewicz, W.W.M. Allison, *Nuovo Cim. A* **57**, 93 (1968).

[5] G. Rinaudo *et al.* [BDNPT Collaboration], *Nucl. Phys. B* **25**, 351 (1971).

[6] J.E. Brau *et al.*, *Phys. Rev. Lett.* **27**, 1481 (1971).

[7] K. Bösebeck *et al.* [ABBC and ABBCCW collaborations], *Nucl. Phys. B* **28**, 381 (1971); **40**, 39 (1972); J.V. Beaupré *et al.* [ABBC and NPT collaborations], *Nucl. Phys. B* **66**, 93 (1973).

[8] L. Van Hove, Proc. IV Int. Symp. on Multiparticle Hadrodynamics, eds. A. Giovannini, S. Ratti, Pavia 1973.

[9] J.J. Engelen *et al.* [ACNO Coll.], *Nucl. Phys. B* **167**, 61 (1980).

[10] B. Kahn, G.E. Uhlenbeck, *Physica* **5**, 399 (1938).

[11] K. Huang, *Statistical Mechanics*, John Wiley and Sons, 1963.

[12] A.H. Mueller, *Phys. Rev. D* **4**, 150 (1971).

[13] M.G. Kendall, A. Stuart, *The Advanced Theory of Statistics*, Vol. 1, C. Griffin and Co., London 1969.

[14] A. Bialas, R. Peschanski, *Nucl. Phys. B* **273**, 703 (1986); **308**, 857 (1988).

[15] A. Bialas, *Multiparticle Dynamics*, Festschrift L. Van Hove, eds. A. Giovannini, W. Kittel, World Scientific, Singapore 1990, p. 75.

[16] E.A. De Wolf, I.M. Dremin, W. Kittel, *Phys. Rep.* **270**, 1 (1996).

[17] T.H. Burnett *et al.* [JACEE Collaboration], *Phys. Rev. Lett.* **50**, 2062 (1983).

[18] M. Adamus *et al.* [NA22 Collaboration], *Phys. Lett. B* **185**, 200 (1987).

[19] Ya.B. Zeldovich, A.A. Ruzmaikin, D.D. Sokoloff, *The Almighty Chance*, Lecture Notes in Physics, Vol. 20, World Scientific, Singapore 1990.

[20] G. Bédard, *Proc. Phys. Soc.* **90**, 131 (1967); D. Cantrell, *Phys. Rev. A* **1**, 672 (1970).

[21] W. Kittel, E.A. De Wolf, *Soft Multihadron Dynamics*, World Scientific, 2005.

[22] P. Lipa, B. Buschbeck, *Phys. Lett. B* **223**, 465 (1989); R. Hwa, *Phys. Rev. D* **41**, 1456 (1990).

[23] A. Bialas, *Nucl. Phys. A* **525**, 345c (1991).

[24] E.K.G. Sarkisyan, *Phys. Lett. B* **477**, 1 (2000); I.G. Abbiendi *et al.* [OPAL Collaboration], *Phys. Lett. B* **523**, 35 (2001).

[25] W. Ochs, J. Wosiek, *Phys. Lett. B* **214**, 617 (1988); **232**, 271 (1989).

[26] I.V. Ajinenko *et al.* [NA22 Collaboration], *Phys. Lett. B* **197**, 457 (1987).

[27] L. Van Hove, *Ann. Phys.* **192**, 66 (1989).

[28] A. Bialas *et al.*, *Phys. Lett. B* **229**, 398 (1989).

[29] N.M. Agababyan *et al.* [NA22 Collaboration], *Phys. Lett. B* **261**, 165 (1991).

[30] C. Albajar *et al.* [UA1 Collaboration], *Nucl. Phys. B* **345**, 1 (1990); B. Buschbeck, *Multiparticle Dynamics*, Festschrift L. Van Hove, eds. A. Giovannini, W. Kittel, World Scientific, Singapore 1990, p. 211; P. Lipa, Ph.D. Thesis, University of Vienna, 1990; P. Lipa *et al.*, Proc. Ringberg Workshop on Multiparticle Production, Ringberg Castle, Germany, 1991, eds. R.C. Hwa, W. Ochs, N. Schmitz, World Scientfic, Singapore 1992, p. 111; N. Neumeister *et al.*, *Z. Phys. C* **60**, 633 (1993); *Acta Phys. Slovaca* **44**, 113 (1994).

[31] A. Capella, K. Fiałkowski, A. Krzywicki, *Phys. Lett. B* **230**, 149 (1989).

[32] D. Seibert, *Phys. Lett. B* **240**, 215 (1990).

[33] M.I. Adamovich *et al.* [EMU-01 Collaboration], *Phys. Rev. Lett.* **65**, 412 (1990); *Phys. Lett. B* **263**, 539 (1991); *Z. Phys. C* **49**, 395 (1991); *Nucl. Phys. B* **388**, 3 (1992); *Phys. Lett. B* **407**, 92 (1997).

[34] B. Wosiek *et al.* [KLMM Collaboration], Proc. XXV Int. Symp. on Multiparticle Dynamics, Stara Lesná 1995, eds. D. Bruncko, L. Šándor, J. Urbán, World Scientific, Singapore 1996, p. 271.

[35] L. Verluyten *et al.* [WA59 and E180 collaborations], *Phys. Lett. B* **260**, 456 (1991).

[36] T. Åkesson *et al.* [HELIOS Collaboration], *Phys. Lett. B* **252**, 303 (1990).

[37] H.G.E. Hentschel, I. Procaccia, *Physica D* **8**, 435 (1983); P. Grassberger, *Phys. Lett. A* **97**, 227 (1983).

[38] N. Agababyan *et al.* [NA22 Collaboration], *Z. Phys. C* **59**, 405 (1993); M. Charlet, Ph.D. Thesis, Nijmegen 1994.

[39] P. Carruthers, I. Sarcevic, *Phys. Rev. Lett.* **63**, 1562 (1989).

[40] H.C. Eggers *et al.*, *Phys. Rev. D* **48**, 2040 (1993); M. Charlet, Proc. XXIII Int. Symp. on Multparticle Dynamics, Aspen 1993, eds. M.M. Block, A.R. White, World Scientific, Singapore 1994, p. 302.

[41] F. Mandl, B. Buschbeck in: Proc. Cracow Workshop on Multiparticle Production, eds. A. Bialas *et al.*, World Scientific, Singapore 1994, p. 1.

[42] N.M. Agababyan *et al.* [NA22 Collaboration], *Phys. Lett. B* **332**, 458 (1994).

[43] M.R. Adams *et al.* [E665 Collaboration], *Phys. Lett. B* **335**, 535 (1994).

[44] A. Bialas, *Nucl. Phys. A* **545**, 285 (1992); *Acta Phys. Pol. B* **23**, 561 (1992).

[45] P. Bak, C. Tang, K. Wiesenfeld, *Phys. Rev. Lett.* **59**, 381 (1987); P. Bak, K. Chen, *Scientific American* **264**, 46 (1991).

[46] W. Kittel, *Acta Phys. Pol. B* **32**, 3927 (2001).

[47] G. Alexander, *Rep. Prog. Phys.* **66**, 481 (2003).

[48] S.V. Akkelin, Yu.M. Sinyukov, *Phys. Lett. B* **356**, 525 (1995); *Z. Phys. C* **72**, 501 (1996).

[49] N.M. Agababyan *et al.* [NA22 Collaboration], *Z. Phys. C* **71**, 405 (1996).

[50] M. Acciari *et al.* [L3 Collaboration], *Phys. Lett. B* **458**, 517 (1999); P. Abreu *et al.* [DELPHI Collaboration], *Phys. Lett. B* **471**, 460 (2000); G. Abbiendi *et al.* [OPAL Collaboration], *Eur. Phys. J. C* **16**, 423 (2000); A. Heister *et al.* [ALEPH Collaboration], CERN-EP/2003-079.

[51] S. Chekanov *et al.* [ZEUS Collaboration], *Phys. Lett. B* **583**, 231 (2004).

[52] C. Adler *et al.* [STAR Collaboration], *Phys. Rev. Lett.* **87**, 082301 (2001); J. Adams *et al.* [STAR Collaboration], *Phys. Rev. Lett.* **93**, 012301 (2004) [arXiv:nucl-ex/0312009].

[53] N.M. Agababyan *et al.* [NA22 Collaboration], *Phys. Lett. B* **422**, 359 (1998); A. Ster, T. Csörgő, B. Lörstad, *Nucl. Phys. A* **661**, 419 (1999); M. Csanád, T. Csörgő, B. Lörstad, A. Ster, *Acta Phys. Pol. B* **35**, 191 (2004); *Nukleonika* **49**, S49 (2004) arXiv:nucl-th/0402037; *Acta Phys. Hung. A* **24**, 139 (2005) [arXiv:hep-ph/0406042].

[54] T. Csörgő, S. Hegyi, W.A. Zajc, *Eur. Phys. J. C* **36**, 67 (2004).

[55] H. Beker *et al.* [NA44 Collaboration], *Z. Phys. C* **64**, 209 (1994);
I.G. Bearden *et al.*, *Phys. Rev. Lett.* **87**, 112301 (2001); S.V. Afanasiev *et al.*
[NA49 Collaboration], *Phys. Lett. B* **557**, 157 (2003).

[56] J. Adcox *et al.* [PHENIX Collaboration], *Phys. Rev. Lett.* **88**, 192302 (2002);
S.S. Adler *et al.*, *Phys. Rev. Lett.* **93**, 152302 (2004)
[arXiv:nucl-ex/0401003]; B.B. Back *et al.* [PHOBOS Collaboration],
*J. Phys. G* **30**, S1049 (2004) [arXiv:nucl-ex/0406027].

[57] B. Lörstad, O.G. Smirnova, Proc. 7th Int. Workshop on Multiparticle
Production, eds. R.C. Hwa *et al.*, World Scientific, Singapore 1997, p. 42.

[58] T. Csörgő, J. Zimányi, *Nucl. Phys. A* **517**, 588 (1990).

[59] A. Bialas, K. Zalewski, *Acta Phys. Pol. B* **30**, 359 (1999).

[60] N.M. Agababyan *et al.* [NA22 Collaboration], *Z. Phys. C* **68**, 229 (1995).

[61] P. Achard *et al.* [L3 Collaboration], *Phys. Lett. B* **540**, 185 (2002).

[62] H. Bøggild *et al.* [NA44 Collaboration], *Phys. Lett. B* **455**, 77 (1999);
I.G. Bearden *et al.*, *Phys. Lett. B* **517**, 25 (2001).

[63] N.N. Aggarwal *et al.* [WA98 Collaboration], *Phys. Rev. Lett.* **85**, 2895 (2000).

[64] J. Adams *et al.* [STAR Collaboration], *Phys. Rev. Lett.* **91**, 262301 (2003).

[65] M.A. Braun, F. del Moral, C. Pajares, *Phys. Lett. B* **551**, 291 (2003).

[66] D. Miskowiec *et al.* [E877 Collaboration], *Nucl. Phys. A* **590**, 473c (1995);
M.A. Lisa *et al.* [E895 Collaboration], *Phys. Lett. B* **496**, 1 (2000).

[67] J. Adams *et al.* [STAR Collaboration], *Phys. Rev. Lett.* **93**, 012301 (2004).

[68] P. Achard *et al.* [L3 Collaboration], *Eur. Phys. J. C* **71**, 1648 (2011);
T. Novák, Ph.D. Thesis, Nijmegen 2008.

[69] V. Khachatryan *et al.* [CMS Collaboration], *J. High Energy Phys.* **1105**, 029
(2011).

[70] R. Astaloš [ATLAS Collaboration], Ph.D. Thesis, 2015, Nijmegen,
Bratislava; W.J. Metzger, arXiv:1512.04301 [hep-ex].

[71] A. Bialas, M. Kucharczyk, H. Palka, K. Zalewski, *Phys. Rev. D* **62**, 114007
(2000).

[72] T. Csörgő, W. Kittel, W.J. Metzger, T. Novák, *Phys. Lett. B* **663**, 214
(2008); W.J. Metzger, T. Novák, W. Kittel, T. Csörgő, *Int. J. Mod. Phys. E*
**16**, 3224 (2008).

[73] P. Dahlqvist, B. Andersson, G. Gustafson, *Nucl. Phys. B* **328**, 76 (1989);
G. Gustafson, A. Nilsson, *Nucl. Phys. B* **355**, 106 (1991); *Z. Phys. C* **52**, 533
(1991).

[74] R. Metzler, J. Klafter, *Phys. Rep.* **339**, 1 (2000).

[75] T. Csörgő, S. Hegyi, W.A. Zajc, *Eur. Phys. J. C* **36**, 67 (2004).

[76] J.P. Nolan, http://fs2.american.edu/jpnolan/www/

[77] A. Bialas, K. Zalewski, *Phys. Lett. B* **727**, 182 (2013); A. Bialas,
W. Florkowski, K. Zalewski, *Phys. Lett. B* **748**, 9 (2015).

[78] N.M. Agababyan *et al.* [NA22 Collaboration], *Phys. Lett. B* **422**, 359 (1998).

[79] A. Ster, T. Csörgő, *AIP Conf. Proc.* **828**, 572 (2006).

[80] A. Ster, T. Csörgő, B. Lörstad, *Nucl. Phys. A* **661**, 419 (1999).

[81] T. Csörgő, *Central Eur. J. Phys.* **2**, 556 (2004) [arXiv:nucl-th/9809011].

[82] T. Novák, T. Csörgő, http://www.kfki.hu/~csorgo/L3/plots/movie.gif and http://www.kfki.hu/~csorgo/L3/plots/Sxyt.gif

[83] Š. Todorova-Nová, *Phys. Rev. D* **89**, 015002 (2014); **86**, 034001 (2012); Quantum Properties of QCD String Fragmentation, XLV Int. Symp. on Multiparticle Dynamics, Wildbad Kreuth, 2015.

[84] B. Andersson *et al.*, *J. High Energy Phys.* **9809**, 014 (1998).